High-Precision Robust Broadband Ultrasonic Location and Orientation Estimation

J. R. Gonzalez and C. J. Bleakley

***Abstract*—This paper presents an indoor broadband ultrasonic system for estimation of a mobile device's 3-D location and three-axis orientation using beacons. It presents the first implementation and characterization of a real frequency hopping spread spectrum-based ultrasonic positioning system, a novel application of uniform circular array angle of arrival estimation techniques to indoor location-orientation estimation and a novel hybrid algorithm for location-orientation estimation. The performance of the system was assessed experimentally. The system has been shown to provide better accuracy, robustness to noise and multipath than other previously reported indoor ultrasonic location or orientation estimation systems with comparable range in the typical office environment tested. The prototype provided location estimates with an error of less than 1.5 cm and and error of less than 4.5° in the yaw, 3° in the pitch and 3.5° in the roll, in 95% of cases.**

***Index Terms*—Angle of arrival, location estimation, orientation estimation, time of arrival, ultrasound.**

I. Introduction

THE commercial success of mobile computing and communications has stimulated research interest in ubiquitous computing—the idea that humans will interact with a wide variety of small computing devices in their everyday lives [1]. Context-aware computing has been proposed as a method for facilitating interaction between man and machine whereby devices sense the user's context and respond appropriately [2]. Clearly, a key element of context is the user's location. Herein, we content that a user's orientation is of similar importance. For example, it is often desirable that systems react differently based on what the user is pointing at or looking towards, even though the user's location is the same. Thus, a system which jointly determines location and orientation is desirable. In addition to providing high accuracy, such a system must be robust to typical impairments such as transducer directionality, noise, and multipath. A high update rate allows the system to respond to movement or gestures. Applications include indoor navigation [3], body-tracking [4], [5], 3-D human computer interfaces [6], and robot navigation [7].

In this paper, a novel system for mobile device (MD) location and orientation estimation in indoor environments is proposed. The system architecture is comprised of a set of fixed base stations (BSs), at known positions, which transmit broadband ultrasonic signals that are acquired by the mobile device. A radio frequency (RF) synchronization signal is provided to the BSs and MD. The MD processes the ultrasonic signals to estimate the time of flight (ToF) and angle of arrival (AoA) of the signals. AoA estimation is performed using a uniform circular array (UCA) of ultrasonic transducers. Based on these estimates, the MD determines its own location and orientation within the reference coordinate system. Since the MD determines its own position, user privacy is maintained. Ultrasonic signals were chosen since they have advantages over radio frequency (RF) signals for the indoor private location applications considered herein. The most important advantages are low propagation velocity and zero leakage between rooms.

The proposed system differs from previous work on ultrasonic location and orientation systems in a number of ways. The paper provides the first experimental comparison of frequency hopped spread spectrum (FHSS), direct sequence spread spectrum (DSSS), and impulsive signaling for indoor location systems. Previous authors have considered DSSS and impulsive-based systems, but not FHSS based systems. This novel use of FHSS is shown to provide accuracy and robustness advantages due to the modulation's inherent robustness to multipath and the well-known near-far problem, as confirmed in simulations reported in [8], [34], and [9]. To the authors' knowledge, this is the first paper to describe the application of array signal processing to the problem of orientation estimation in an indoor ultrasonic system. In order to provide for efficient estimation, modal-decomposition acoustic theory is applied to the AoA estimation problem. The MUSIC algorithm, presented in [10], is extended to allow for the use of broadband signals and a UCA. MUSIC was chosen since it provides better performance than other methods at lower computational cost [10]. It also uses real-valued operations rather than complex, reducing its computational complexity. A novel algorithm is presented which estimates location and orientation within a given reference frame based on the raw ToF and AoA estimates at the MD. The method is found to be accurate, providing good robustness to error in the ToF and AoA estimates. To the authors' knowledge, this is the first paper to use vector rotation formalisms in a location-orientation estimation system. The performance of the proposed algorithms and techniques was assessed experimentally using a prototype system. The system provides location and orientation estimation accuracy and robustness in excess of any previously reported ultrasonic system with similar range.

This paper is structured as follows. Previous location and orientation work is described in Section II. Section III-A introduces the spread spectrum modulation techniques considered

Manuscript received June 29, 2008; revised April 14, 2009. Current version published October 21, 2009. This work was supported by a research grant from Science Foundation Ireland. The associate editor coordinating the review of this manuscript and approving it for publication was Dr. Fredrik Gustafsson.

The authors are with the School of Computer Science and Informatics, Complex and Adaptive Systems Laboratory, University College Dublin, Clonskeagh, Dublin 4, Ireland (e-mail: juan.gonzalez-hernandez@ucdconnect.ie; chris.bleakley@ucd.ie).

Color versions of one or more of the figures in this paper are available online at http://ieeexplore.ieee.org.

Digital Object Identifier 10.1109/JSTSP.2009.2027795

herein. Section III-B introduces Modal Array Signal Processing and explains the background theory for the AoA estimation algorithms as well as the UCA-RB-MUSIC algorithm on which the proposed estimation method is based. Section IV presents the proposed algorithms and techniques. Section IV-A describes the proposed modulation, Section IV-B explains the method for robust ToF estimation used herein and Section IV-C presents the proposed AoA estimation method and a study of the error arising due to the use of the far-field assumption. Section IV-D describes the proposed location-orientation estimation algorithm. Section V describes the prototype developed to assess the performance of the algorithms. Results are provided in Section VI and conclusions and further work are included in Section VII.

II. Related Work

This section presents previous location and orientation systems. Ultrasonic location estimation has been widely studied. Hence, only the most relevant works are described. For a more complete overview, see [11]. Orientation estimation has been studied much less. Few of the systems described previously consider the problems of ultrasonic orientation estimation or of estimation in an indoor environment. Relevant work is presented herein, as well as a historical review of the most important algorithms for rotation manipulation, which are the basis of one of the proposed algorithms.

A. Ultrasonic Location Systems

The Bats system, presented in [12], consists of MDs, each with an RF receiver and an ultrasonic transmitter. Ultrasonic sensors are placed at known positions on the ceiling of a room. These sensors are connected to a central server, which periodically sends a RF pulse. On receiving this pulse, all of the Bat units emit an ultrasonic pulse. The receivers in the room measure the ToF of these signals. With at least three measurements, the 3-D position of the MD can be calculated using a multilateralization algorithm. One of the system's biggest problems is that, since the Bats emit single ultrasonic pulses, multipath and noise can severally degrade system performance. Also, the server must wait for echoes to die down before resending the RF pulse. This reduces the update rate and prevents motion tracking. Since it is a centralized architecture, the privacy of Bats' users is not preserved.

The Cricket system, presented in [13], consists of beacons in the ceiling and a receiving MD. The beacons periodically transmit an ultrasonic pulse and a simultaneous RF pulse. The MD measures the ToF of the ultrasonic signals. As with Bats, the system has poor robustness to multipath and noise and a low update rate. In tests, the system provided 3-D location estimates with an error of 5 to 25 cm, which is unacceptable for many ubiquitous computing applications.

The system presented in [14] and [15] is important because it was one of the few ultrasonic location systems that uses broadband signals. Broadband ultrasonic transmitters were placed at known locations on the ceiling and transmit simultaneously with RF synchronization. The DSSS modulation used allows multiple transmitters to send simultaneously with separation of the signals at the MD. When at least three signals are available to the MD, a multilateralization method is used by the MD to estimate its own position. While DSSS provides greater robustness than previous impulsive systems, the system suffers from the near-far problem whereby signals from nearby beacons overwhelm signals from distant beacons, preventing location estimation. Furthermore, the transducers used are highly customized and not commercially available.

The Whisper system [16], also uses SS techniques. Its most significant advance is the use of a Kalman filter to track the ToF of the received signals.

B. Orientation Systems

Some existing orientation estimation systems, such as [17], infer orientation using location estimates from several sensors. The most important disadvantage of this kind of system is that, in order to minimize the error in orientation estimation arising from errors in the location estimates, the sensors have to have a large separation, which is unacceptable for some applications.

One of the most important orientation estimation systems was presented in [18]. In this work, an electronic compass was added to the Cricket system to provide orientation estimates. The system uses an antenna array to estimate the azimuth of the MD. The problem with the system is that the greater the angle estimated, the less accurate the estimate. That is partially due to elevation ambiguity. Azimuth estimation error increases from < 1 to 20° as elevation goes from 0 to 90°. Other systems, such as [19] and [20], estimate orientation using specific hardware, such as TILT technology. These systems provides a narrow range of angle estimates, as well as poor accuracy.

In this work, orientation estimation uses vector rotations in various coordinate systems. The mathematical basis for this was established in 1959, when Thompson published a first solution for rotation between two coordinate systems [21]. Later, Schut employed quaternations to reduce the computational cost of the algorithm. Other variations of Thompson's work focused on reducing the computational cost of the rotation matrix [22] and [23]. Further studies, such as [24] and [25], provided closed-form solutions.

III. Background on Spread Spectrum Signalling and Array Processing

A. Spread Spectrum Modulation

Spread Spectrum (SS) modulations have been shown to provide robustness to multipath and noise and allow simultaneous transmission [8], [26], [27] and [9]. For these reasons, they are attractive for use in ultrasonic location systems. A SS signal is, as was defined in [26], a signal that has an extra modulation that expands the signal bandwidth beyond what is required by the underlying data modulation. The expansion process is called spreading, and it is often performed using a *pseudorandom binary sequence*, which is defined in [27] as a stochastic process that consists of independent, identically distributed symbols, each of duration T. Each symbol takes the value $+1$ or -1 with equal probability. These sequences are grouped in orthogonal sets, which allow simultaneous transmission by more than one transmitter.

1) Direct Sequence Spread Spectrum: Direct Sequence Spread Spectrum is a very popular SS modulation where the original data is spread using a pseudorandom sequence with a higher rate. The data and the sequence are bipolar $(-1, 1)$ and the spreading is done by multiplying the signals. The resulting signal is modulated, usually by a phase modulation, such as binary phase shift keying (BPSK) or quadrature phase shift keying (QPSK). The signal of user k is given by [27]

$$x^{(k)}(t) = d^{(k)} \sum_{l=0}^{L-1} c_l^{(k)} pT_c(t - lT_c), \quad 0 \le t < T_d \tag{1}$$

where T_d is the data period, T_c is the chip period, and $L = T_d/T_c$ is the chipping rate; $d^{(k)}$ is the transmitted data symbol of user k, the rectangular pulse $pT_c(t)$ is equal to 1 for $0 \le t < T_c$ and zero otherwise. T_c is the chip duration and $c_l^{(k)}$ are the chips of the user k spreading sequence $c_{(k)}(t)$.

At the receiver, the signal is firstly demodulated and then multiplied by the spreading code to despread the signal. DSSS is very efficient spectrally and has fairly straightforward synchronization requirements. One of its disadvantages is that, in order to spread the signal, the rate must be increased, leading to an increase in implementation complexity and cost. Furthermore, DSSS is more sensitive to impulsive and frequency selective distortions than FHSS [27].

2) Frequency-HOP Spread Spectrum: In FHSS, the signal is spread using a carrier frequency that hops between a set of frequencies, depending on a pseudorandom sequence. There are two FHSS techniques—Fast and Slow. Fast FHSS uses several frequency hops per bit. In contrast, Slow FHSS uses one hop for several data bits. The main differences between Slow and Fast FHSS are interference rejection and electronic complexity [28], [29]. Fast FHSS is sensitive to timing or synchronization errors and the modulator and demodulator electronics are more complex because of the higher hopping rate. On the other hand, the interference rejection of Fast FHSS is better than that of Slow FHSS [28].

In both cases, the data signal is modulated using FSK or BPSK. Next, the signal is spread using a sinusoidal signal with variable frequency depending on the pseudorandom code. The demodulator firstly despreads the signal and then demodulates it. The following equation describes FHSS modulation [27]:

$$x^{(k)}(t) = d^{(k)} P_{T_b}(t) \sin(2\pi f_m t + \phi) \tag{2}$$

where T_b is the data symbol duration, $d^{(k)}$ is the transmitted data symbol of user k, the rectangular pulse $pT_b(t)$ is equal to 1 for $0 \le t < T_b$ and zero otherwise, and f_m is the set of frequencies over which the signal hops. One of the main advantages of FHSS over other modulations is that, due to its variable carrier frequency, only noise and multipath in the same band of frequencies as the signal affects it. Furthermore, the data rate is not increased by the spreading. However, the modulation is less spectrally efficient, the electronics are more complex and it has more stringent synchronization requirements.

B. Array Signal Processing

This section presents an introduction to array signal processing focused on the modal decomposition of acoustic signals for UCA-MUSIC. The study focuses on uniform circular arrays, which were used in this work. For a broader introduction to array signal processing and sound wave harmonic decomposition, the reader is referred to [30]–[32], and [33].

Consider a set of N_S signals impinging on an array, with direction $[\phi_n, \theta_n], n = 1, \ldots N_S$. The received signal at each sensor at an instant n is called *the snapshot* and is defined in [32] as

$$\underline{X}_n = \underline{\underline{A}}\underline{S} + \underline{w}_n \tag{3}$$

$$\underline{S} = \begin{bmatrix} S_1(n) \\ S_2(n) \\ \vdots \\ S_{NS}(n) \end{bmatrix}$$

$$\underline{\underline{A}} = [\underline{a}_1(\varsigma_1, \phi_1), \underline{a}_2(\varsigma_2, \phi_2) \ldots, \underline{a}_{NS}(\varsigma_{NS}, \phi_{NS})] \tag{4}$$

where $S_i(n)$ is the complex envelope of each of the N_S signals at time n, $\underline{\underline{A}}$ is a matrix containing the AoA of each signal, and $\underline{w}_n$ is independent White Gaussian noise at each sensor. The snapshot is basically, the sum of contributions of a set of sources plus noise.

The AoA information is included in the phase difference between sensors. The covariance matrix is obtained by calculating the correlations between all the sensors and placing the results in a $M \times M$ matrix, where M is the number of sensors in the array.

$$\underline{\underline{R}} = E\left[X_n \cdot X_n^H\right]. \tag{5}$$

The covariance matrix R is defined in (5). In practical applications, the number of observations is limited, so, using a number of snapshots, N_{snap}, the covariance matrix is estimated according to

$$\underline{\underline{\hat{R}}} = \frac{1}{N} \sum_{q=0}^{N_{snap}-1} X_{n-q} X_{n-q}^H. \tag{6}$$

The UCA-RB-MUSIC algorithm is based on employing a beamformer F_r^H to map the manifold vector $\underline{a}(\varsigma, \phi)$, defined for NS signals in (7), to a real-valued manifold vector $\underline{b}(\varsigma, \phi)$

$$\underline{a}(\varsigma, \phi) = \begin{bmatrix} e^{i\varsigma_1 \cos(\phi_1 - \gamma_0)} & \ldots & e^{i\varsigma_{NS} \cos(\phi_{NS} - \gamma_0)} \\ e^{i\varsigma_1 \cos(\phi_1 - \gamma_1)} & \ldots & e^{i\varsigma_{NS} \cos(\phi_{NS} - \gamma_1)} \\ \vdots & \ldots & \vdots \\ e^{i\varsigma_1 \cos(\phi_1 - \gamma_{N-1})} & \ldots & e^{i\varsigma_{NS} \cos(\phi_{NS} - \gamma_{N-1})} \end{bmatrix}. \tag{7}$$

The beamforming matrix F_e^H, which is necessary to generate the beamformer F_r, is defined as follows:

$$\begin{aligned} F_e^H &= C_e V^H \\ C_e &= diag\left\{j^{-M_{\mathrm{mod}}}, \ldots, j^{-1}, j^0, j^1, \ldots, j^{M_{\mathrm{mod}}}\right\} \\ V &= \sqrt{M}\left[w_{-M_{\mathrm{mod}}} \vdots \cdots \vdots w_0 \vdots \cdots \vdots w_{M_{\mathrm{mod}}}\right] \end{aligned} \tag{8}$$

where M is the number of sensors, $w_m^H = 1/M\left[e^{jm\gamma_0}, e^{jm\gamma_1}, \ldots, e^{jm\gamma_{M-1}}\right]$ and M_{mod} denotes the maximum excitation mode of the array, which can be calculated as explained in [10] by $M_{\mathrm{mod}} \approx k_0 r$, where r is the

radius of the array and $k_0 = 2\phi\lambda$. Let us define the beamformer F_r and the associated manifold vector as follows:

$$F_r^H = W^H F_e^H = W^H C_e V^H \tag{9}$$

$$a_r(\Theta) = F_r^H \underline{a}(\Theta) = W^H a_e(\Theta) \approx \sqrt{M} W^H J(\varsigma) v(\theta). \tag{10}$$

It is easy to see that the beamspace $a_r(\Theta)$ is real-valued if the matrix W^H has centro-Hermitian rows. The orthogonality of F_r^H is maintained by restricting W to be unitary. The sparse matrix W is defined as follows:

$$W^H = \frac{1}{\sqrt{2}} \begin{bmatrix} I_{M_{\mathrm{mod}}} & 0_{M_{\mathrm{mod}}} & \tilde{I}_{M_{\mathrm{mod}}} \\ 0^T_{M_{\mathrm{mod}}} & \sqrt{2} & 0^T_{M_{\mathrm{mod}}} \\ jI_{M_{\mathrm{mod}}} & I_{M_{\mathrm{mod}}} & -j\tilde{I}_{M_{\mathrm{mod}}} \end{bmatrix} \tag{11}$$

where $0_{M_{\mathrm{mod}}}$ denotes a zero vector of length M_{mod}.

Let $A = [a(\Theta_1), \ldots, a(\Theta_N S)]$ be the $M \times NS$ AoA matrix, assuming N_S signals arriving at the sensors. Using the typical covariance matrix representation, we employ the beamformer F_r^H to build the real-valued beamspace AoA matrix R_y as follows:

$$R_y = F_r^H R F_r = A_r P A_r^T + \sigma_\eta^2 I$$
$$R = \Re\{R_y\}. \tag{12}$$

Let S and G be the matrices spanning the beamspace signal and noise subspaces, respectively:

$$S = [s_1, \ldots, s_d]$$
$$G = [g_{d+1}, \ldots, g_{M'}]. \tag{13}$$

The UCA-RB-MUSIC spectrum is defined as

$$S_{\mathrm{UCA-RB-MUSIC}}(\Theta) = \frac{1}{a_r^T(\Theta) G G^T a_r(\Theta)} \tag{14}$$

which has peaks at the signal arrival directions. AoA estimates are obtained by searching for N_S peaks in the 2-D spectrum.

IV. Proposed Ultrasonic Location-Orientation Algorithm

This section describes the proposed ultrasonic location-orientation algorithm.

A. Spread Spectrum Modulation

In Section III-A, both DSSS and FHSS were presented. Spread Spectrum modulation requires synchronization between the received signal and the spreading code to despread the signal. Depending on the modulation, this synchronization is more or less restrictive. The goal of synchronization in location systems is to determine the delay between the *received* signal and the *transmitted* signal, in order to determine the ToF of the signal in an accurate and reliable way.

In previous simulation studies [34], [42], the authors' demonstrated that FHSS outperforms DSSS in terms of robustness in location systems. This confirmed similar results in communication studies [9]. In this paper, the data signal is generated using a Kasami orthogonal code [35]. As can be seen in Table I, Kasami codes provide the best autocorrelation peak and ratio between maximum auto and cross-correlation. Background on m-sequences, Gold and Golay codes can be found in [36], [37], and [38].

TABLE I
Sequences Performance for 32 Length and Aperiodic Correlation.

Code	Max of autocorr	Relative max autocorr	Max of crosscorr
m-sequence	13	7	9
Gold	14	7	8
Kasami	15	7	9
Golay	14	9	10

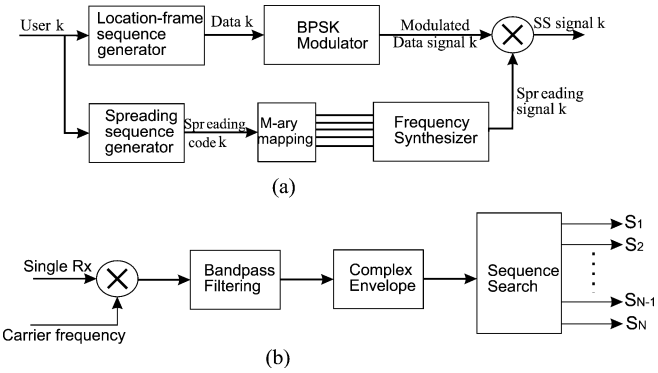

Fig. 1. Schematics. (a) Transmitter. (b) Receiver.

The transmitter modulation scheme is shown in Fig. 1(a). User k (BS k) uses a Kasami code as data, modulating the carrier using BPSK. A second Kasami code is used to generate the hopping pattern with which the signal is spread using FHSS. The user k, (BS_k) is defined in the system by two sequences, one to build the data and another to spread the signal.

In order to provide a clear cross-correlation peak, a data frame consist of a Kasami code of 50 chips, with a chip duration of 0.2 ms, and 16 cycles of the carrier per chip. The generated signal has a bandwidth of 2.5 kHz. The *spreading sequence* is generated and mapped to M symbols, where M is the number of hops allowed. In the proposed implementation, six hops were used for a final bandwidth of 15 kHz which was consistent with the bandwidth of the transducer. The mapped sequence is sent to a frequency synthesizer that converts it to a sinusoid of variable frequency. The modulated data frame is multiplied by this signal to generate a final signal, which consists of a BPSK signal with a variable carrier frequency. The longer the frame, the better the cross-correlation peak, but the lower the update rate. The hop duration was chosen to avoid early multipath. Early multipath is produced by near reflectors, which give rise to path delays close to that of the direct path. Early multipath can cause collisions in all hops, severely degrading system performance. In the present work, a hop duration of 250 μs was chosen, providing robustness against early reflectors at 8.6 cm. The number of hops was chosen so as to allow protection from late multipath.

Due to the use of orthogonal spreading sequences, several transmitters can send signals at the same time. The demodulator receives a combination of the transmitted signals, multipath interference and noise. The receiver first multiplies the received signal by a sinusoid whose frequency is the central frequency of

the transmitted signals. Next, a filtering step is applied, leaving only the baseband signal.

It is worth noting that data transmission is not required, the goal is accurate ToF estimation by peak picking of the cross-correlation output. The use of the Kasami code as data allows an efficient separation of the signals from each BS providing a clear and accurate cross-correlation peak to estimate the ToF.

In BPSK, the frequency components can be described by the Fourier transform of a delayed pulse. Let us call this the data pulse chip, as it is usual in the literature. The frequency representation of a chip is as follows:

$$\operatorname{sinc}(x) = \begin{cases} \frac{\sin(\pi x)}{\pi x} & x \neq 0 \\ 1 & x = 0 \end{cases} \tag{15}$$

where x is the ratio between the represented frequency and the chip frequency. The points where the signal crosses the horizontal axis are the frequency inverses of the chip period. The chip period is determined by

$$\frac{1}{T_{\text{chip}}} = \frac{f_c}{n_{\text{cycles}}} \tag{16}$$

where f_c is the carrier and n_{cycles} the number of carrier frequency cycles per chip. With FHSS, the carrier frequency hops between a set of frequencies, which means that the number of chips per cycle is variable depending on the carrier frequency.

Let us assume M_{hop} hops. The maximum chip bandwidth is then B/M_{hop}, where B is the available bandwidth. The carrier frequencies are then

$$\left[f_1 + \frac{B}{2M_{\text{hop}}}, f_1 + \frac{3B}{2M_{\text{hop}}}, \ldots, f_2 - \frac{B}{2M_{\text{hop}}} \right] \tag{17}$$

where f_1 and f_2 are the lower and upper boundaries of the frequency range. The maximum carrier frequency is defined as $f_c|_{\max} = f_2 - B/2M_{\text{hop}}$ and the number of hops per chip are

$$n_{\text{cycles}} = f_c|_{\max} \cdot T_{\text{chip}} = \frac{f_c|_{\max} \cdot M_{\text{hop}}}{B} \tag{18}$$

$$n_{\text{cycles}} = \text{round}\left[\frac{f_2 \cdot M_{\text{hop}}}{B} - \frac{1}{2} \right]. \tag{19}$$

B. Time-of-Flight (ToF) Estimation

The ToF estimation algorithm is based on measuring the similarity between the *received* signal and the *expected* signal. The similarity measure used is the cross-correlation of the signals x and y, respectively,

$$R_{xy}(m) = E\{x_{n+m} y_n^*\} = E\{x_n y_{n-m}^*\}$$
$$\hat{R}_{xy}(m) = \begin{cases} \sum_{n=0}^{N-m-1} x_{n+m} y_n^* & m \geq 0 \\ \hat{R}_{yx}^*(-m) & m < 0 \end{cases}. \tag{20}$$

As can be seen in Fig. 2(a), the raw cross-correlation function has multiple peaks due to the carrier sinusoids. To obtain a more reliable estimate, we calculated the complex envelope of the cross-correlation output, defined as

$$\tilde{X} = X + j\hat{X} \tag{21}$$

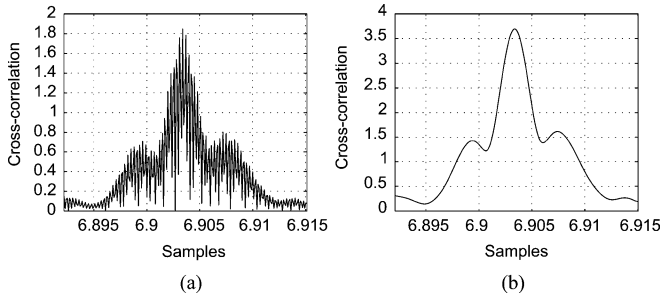

Fig. 2. Cross-correlation peak (a) before and (b) after complex envelope.

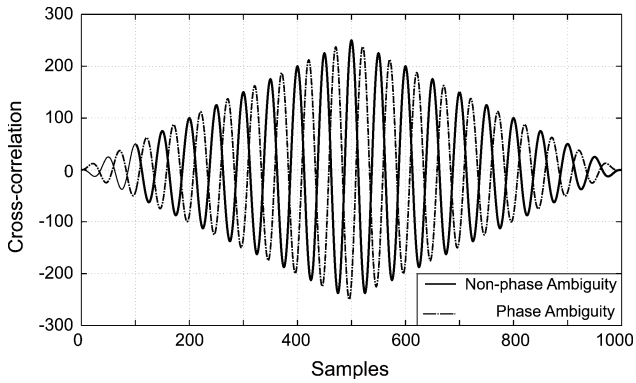

Fig. 3. BPSK phase ambiguity.

where $\hat{X}$ is the Hilbert transform of X. Fig. 2(b) shows the corresponding complex envelope.

Once the ToF has been identified by determining the delay of the maximum of the complex envelope of the cross-correlation function, the MD-BS distance is estimated according to $d = n_{\text{samples}} * c/f_s$ where n_{samples} is the sample number of the maximum, c is the speed of sound and f_s is the sampling frequency. In practical systems, a temperature sensor may be used to correct for the variation of the speed of sound in air with temperature.

Using BPSK signals allows for efficient use of the bandwidth. Unfortunately, a consequence of using BPSK is that the phase of the carrier of the acoustic signals is unknown because it is dependent on the distance between the transmitting and receiving transducers, and the precise wavelength of the carrier frequency (about 8.5 mm for 40-kHz ultrasound in typical indoor conditions). This effect can be seen in Fig. 3, where the solid and dotted lines show the cross-correlation of two sinusoids with the same and different phases, respectively. As can be seen, taking the time of the maximum value as the estimate of ToF can lead to a small error.

The solution proposed herein is to mitigate this effect by parabolic interpolation of the complex envelope of the cross-correlation output. Hyperbolic interpolation is used herein

$$\hat{D}_{\text{interp}} = n_m - \frac{1}{2} \frac{\hat{R}_{xy}[n_{m+1}] - \hat{R}_{xy}[n_{m-1}]}{\hat{R}_{xy}[n_{m+1}] + \hat{R}_{xy}[n_{m-1}] - 2\hat{R}_{xy}[n_m]} \tag{22}$$

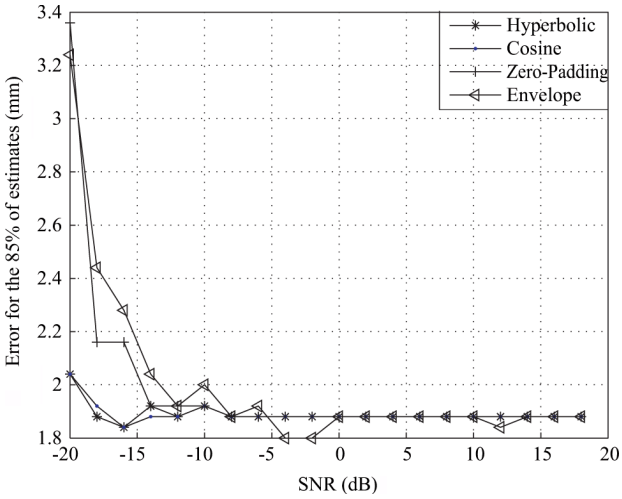

Fig. 4. ToF error for different interpolation functions.

where R_{xy} is the cross-correlation function and n_m is the position of the maximum peak of the cross-correlation. This interpolation was shown in simulation to perform slightly better than cosine, zero padding and envelope interpolation for a typical FHSS signal, as can be seen in Fig. 4. The zero-padding technique consists of introducing regularly zeros in the signals before performing cross-correlation. Envelope interpolation consists of computing the complex-envelope of the signals before correlate them. Cosine interpolation is defined as

$$\begin{aligned} \hat{D}_{\cos} &= n_m - \frac{c}{b} \\ \cos(b) &= \frac{\hat{R}_{xy}[n_m - 1] + \hat{R}_{xy}[n_m + 1]}{2\hat{R}_{xy}[n_m]} \\ \tan(c) &= \frac{\hat{R}_{xy}[n_m - 1] - \hat{R}_{xy}[n_m + 1]}{2\hat{R}_{xy}[n_m]\sin(b)} \end{aligned} \tag{23}$$

where the parameters are the same as for hyperbolic interpolation.

C. Angle-of-Arrival (AoA) Estimation

A signal can considered narrowband when it fulfills the following condition:

$$\frac{B_0}{f_0} \cdot \frac{D}{\lambda} \ll 1 \tag{24}$$

where B_0 is the bandwidth of the signal, f_0 is the center frequency of the signal, D is the diameter of the sensor array, and λ is the wavelength. For the signal parameters used herein, this condition is not met.

The main problem in AoA estimation using broadband signals is that the assumption that the group delay is equal for all the frequencies is wrong. It can be seen in (7) that, in order to compute the array manifold vectors, the spectrum of the beamformer in (14), the value of k_0 and of the carrier frequency are necessary.

Herein, a broadband AoA estimation procedure is used. The fast Fourier transform (FFT) of the signal received at each sensor is computed. The FFT output is separated into

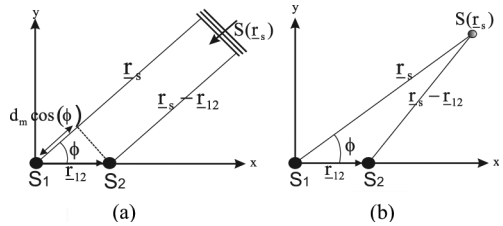

Fig. 5. Signals arriving at an array. (a) Far-field source. (b) Near-field source.

15 frequency bins and 15 AoA estimates are calculated using UCA-RB-MUSIC, each for a bandwidth of 1 kHz. Using this technique, the condition of (24) is met. The final AoA estimate is calculated as the mean of all 15 estimates.

Typically, work done in array signal processing is based on the assumption of a plane wave arriving at the array. The present work is aimed at applications in indoor environments where the distances between the transmitters and the sensor array are short. Because of this, it is necessary to consider the error introduced by making the far field assumption.

Fig. 5 presents two situations: a plane wave and a near-field signal arriving at the array. Two sensors are assumed, with a separation of $d_{12} = \|\underline{r}_{12}\|$. In the far field case the distance $\tilde{d}_{ff}$ is defined as

$$\tilde{d}_{ff} = d - d_{12}\cos(\phi) \tag{25}$$

where $\tilde{d} = \|\underline{r}_S - \underline{r}_{12}\|$, $d = \|\underline{r}_S\|$ and $d_{12} = \|\underline{r}_{12}\|$. The same distance in the near field case is

$$\tilde{d}_{nf}^2 = d^2 - d_{12}^2 - 2dd_{12}\cos(\phi) \tag{26}$$

which, after Taylor series expansion can be expressed as

$$\tilde{d}_{nf}^2 \approx \underbrace{d - d_{12}\cos(\phi)}_{\tilde{d}_{ff}} + \underbrace{\frac{d_{12}^2}{2d}\sin^2(\phi)}_{\varepsilon_{nf}} \tag{27}$$

where ε_{nf} is the approximate error arising from the far field assumption. The maximum error occurs when $\phi = \pi/2$ and, for an aperture with a maximum dimension D

$$\varepsilon_{nf_{\max}} = \frac{D^2}{8d}. \tag{28}$$

Usually, this maximum error is defined relative to a phase error quantified as $1/k_{th}$ of a wavelength. Usually, k is chosen to be 16 [39] so the distance is

$$d|_{\varepsilon_{nf-\max}=\lambda/\kappa} = \frac{D^2}{8\frac{\lambda}{k}} = \frac{kD^2}{16\pi}\kappa \;\kappa > 0. \tag{29}$$

Fig. 6 shows the transition from the near field to the far field, $d_D = \kappa k D/16\pi$, for different error values κ and an aperture size of 1.28 cm, equal to that of the antenna array implemented in the prototype. As can be seen, the distance depends on the frequency of the signal, the aperture size and the acceptable error. Clearly, for the ultrasonic signals under consideration, it is desirable to use small sensors with small separations. Fig. 6 plots the results for an array with eight sensors and a separation of 5.14 mm.

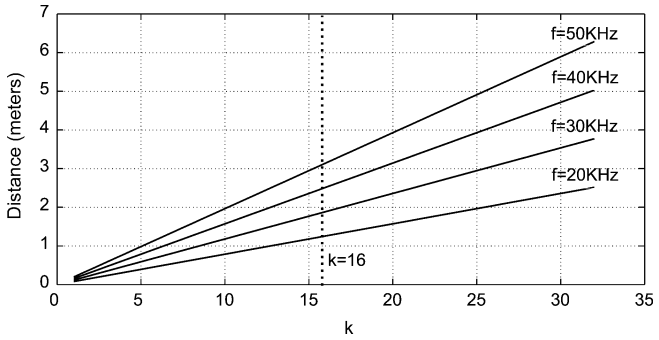

Fig. 6. Distances beyond which the far field condition can be assumed with an given error.

D. Location-Orientation Estimation

This algorithm was previously presented in [42] and [8]. In the first paper, the mathematical approach was explained in detail and in the second simulation results were provided. Herein, the algorithm is tested in a real implementation.

In system operation, a set of M_{BS} Base Stations with known positions $\underline{r}_{\mathrm{BS}_i} = [x_{\mathrm{BS}_i}, y_{\mathrm{BS}_i}, z_{\mathrm{BS}_i}]$ transmit SS signals to the MD at position $\underline{p} = [x_{\mathrm{MD}}, y_{\mathrm{MD}}, z_{\mathrm{MD}}]$. The MD includes an antenna array of M_{sen} sensors. It receives the signals and measures two parameters—ToF and AoA. RF synchronization is assumed between the BSs and MD so that measurements of ToF can be converted to absolute distances, allowing spherical localization. Typical RF modules have jitter of ± 5 ps, which introduces a ToF error equivalent to ± 0.01715 ms. Based on this, radio-frequency synchronization errors are not considered in the analysis.

As input parameters, the location-orientation algorithm takes the set of M_{BS} distances and M_{BS} 2-D angles

$$d_i \quad i = 1 \ldots M_{\mathrm{BS}}$$
$$[\theta_i, \phi_i] \quad i = 1 \ldots M_{\mathrm{BS}} \tag{30}$$

where azimuth $\theta = \arctan\left(z/\sqrt{x^2+y^2}\right)$ and elevation $\phi = \arctan(y/x)$.

The orientation of the MD is defined as $\underline{o} = [x_o, y_o, z_o]$ and can be described using Euler angles and a rotation matrix as follows:

$$\begin{aligned}
R &= \begin{pmatrix} a_{11} & a_{12} & a_{13} \\ a_{21} & a_{22} & a_{23} \\ a_{31} & a_{32} & a_{33} \end{pmatrix} \\
a_{11} &= \cos(y_o)\cos(z_o) \\
a_{12} &= \cos(y_o)\sin(z_o) \\
a_{13} &= -\sin(y_o) \\
a_{21} &= \sin(x_o)\sin(y_o)\cos(z_o) - \cos(x_o)\sin(z_o) \\
a_{22} &= \sin(x_o)\sin(y_o)\sin(z_o) + \cos(x_o)\cos(z_o) \\
a_{23} &= \sin(x_o)\cos(y_o) \\
a_{31} &= \cos(x_o)\sin(y_o)\cos(z_o) + \sin(x_o)\sin(z_o) \\
a_{32} &= \cos(x_o)\sin(y_o)\sin(z_o) - \sin(x_o)\cos(z_o) \\
a_{33} &= \cos(x_o)\cos(y_o).
\end{aligned} \tag{31}$$

The MD's rotation produces a change in the BS positions within the MD's coordinate system, leading in a variation in the estimated angles, so $\hat{\theta} \neq \theta$ and $\hat{\phi} \neq \phi$.

The measured information from each BS is grouped in a vector. Using this vector and the known position of the BSs, the MD location in the BS coordinate system is estimated as $\hat{p}_i = [\hat{x}_{MS_i}, \hat{y}_{MS_i}, \hat{z}_{MS_i}]$, according to

$$\begin{aligned}
x_{MS_i} &= x_{\mathrm{BS}_i} - \hat{d}_i \cos\left(\hat{\phi}_i\right)\cos\left(\hat{\theta}_i\right) \\
y_{MS_i} &= y_{\mathrm{BS}_i} - \hat{d}_i \sin\left(\hat{\phi}_i\right)\cos\left(\hat{\theta}_i\right) \\
z_{MS_i} &= z_{\mathrm{BS}_i} - \hat{d}_i \sin\left(\hat{\theta}_i\right).
\end{aligned} \tag{32}$$

In the error-free case, there is a single MD 3-D orientation that provides a consistent location estimate $\hat{p}$ for all BS information vectors, that is

$$\underline{\hat{p}} = \underline{\hat{p}}_i \cdot \underline{\underline{R}}. \tag{33}$$

The MD location may be determined by rotating the position estimates using the BS locations as center points. Hence, (33) is rewritten as

$$\underline{\hat{p}} = \left(\underline{\hat{p}}_i - \underline{r}_{\mathrm{BS}_i}\right) \cdot \underline{\underline{R}} + \underline{r}_{\mathrm{BS}_i} \tag{34}$$

where $\underline{\hat{p}}_i$ is the MD position estimated by BS_i at $\underline{r}_{\mathrm{BS}_i}$ and $\underline{\hat{p}}$ is the MD position after rotation.

To obtain a MD location which is consistent for all BS measurements, an estimate of the rotation matrix $\underline{\underline{\hat{R}}}$ is necessary. From (34) and (31)

$$\underline{\hat{p}}_i - \underline{r}_{\mathrm{BS}_i} = p_{\mathrm{rel}_i} \quad p_{\mathrm{rel}_i} = [x_{\mathrm{rel}_i}, y_{\mathrm{rel}_i}, z_{\mathrm{rel}_i}] \tag{35}$$

$$\begin{aligned}
\hat{x}_{\mathrm{MD}} - x_{\mathrm{BS}_i} &= x_{\mathrm{rel}_i} a_{11} + y_{\mathrm{rel}_i} a_{12} + z_{\mathrm{rel}_i} a_{13} \\
\hat{y}_{\mathrm{MD}} - y_{\mathrm{BS}_i} &= x_{\mathrm{rel}_i} a_{21} + y_{\mathrm{rel}_i} a_{22} + z_{\mathrm{rel}_i} a_{23} \\
\hat{z}_{\mathrm{MD}} - z_{\mathrm{BS}_i} &= y_{\mathrm{rel}_i} a_{31} + y_{\mathrm{rel}_i} a_{32} + z_{\mathrm{rel}_i} a_{33}.
\end{aligned} \tag{36}$$

These equations define a system of M_{BS} equations which can be solved to obtain three of the $\underline{\underline{R}}$ coefficients and the MD position in one axis.

In order to reduce the number of variables in the system, the MD location is now estimated. For each sensor, a set of BS distances are obtained. Using at least three of these and by applying a Taylor series trilateration method [40], a set of location estimates are obtained, one for each sensor in the array. These location estimates form a circular grid, following the position of the sensors. AoA estimation is performed using the central sensor as a coordinate reference. Because of this, location estimation should be performed relative to the center of the array. By calculating the mean of the 3-D location estimates, the location of the center of the array can be accurately estimated. Estimation accuracy is enhanced because errors are mitigated by means of the redundancy in the system.

This provides the estimate $[\hat{x}_{\mathrm{MD}}, \hat{y}_{\mathrm{MD}}, \hat{z}_{\mathrm{MD}}]$. Regrouping terms, the system can be solved by

$$\begin{aligned}
A &= \begin{bmatrix} x_{\mathrm{rel}_1} & y_{\mathrm{rel}_1} & z_{\mathrm{rel}_1} \\ \cdots & \cdots & \cdots \\ x_{\mathrm{rel}_N} & y_{\mathrm{rel}_N} & z_{\mathrm{rel}_N} \end{bmatrix} \\
B &= \begin{bmatrix} x'_{MD1} - x_{\mathrm{BS1}} \\ \cdots \\ x'_{\mathrm{MDN}} - x_{\mathrm{BS}N} \end{bmatrix}
\end{aligned} \tag{37}$$

where N is the number of BSs available. With a minimum of three BSs, this gives a set of three or more linearly independent equations.

Once $\underline{\underline{R}}$ is estimated, the MD orientation is obtained using

$$\begin{aligned} y_o &= -\arcsin(a_{13}) \\ z_o &= \frac{1}{2}\mathrm{ar}\cos\left(\frac{a_{11}}{\cos(y_{or})}\right) + \frac{1}{2}\arcsin\left(\frac{a_{12}}{\cos(y_{or})}\right) \\ x_o &= \frac{1}{2}\mathrm{ar}\sin\left(\frac{a_{21}}{\cos(y_{or})}\right) + \frac{1}{2}\mathrm{ar}\cos\left(\frac{a_{31}}{\cos(y_{or})}\right). \end{aligned} \quad (38)$$

The computational requirements are not much greater than typical trilateration methods. The method is suitable for real-rime implementation. Assuming a sensor array with M elements and a set of N available BSs, N means over M ToF estimates are necessary, as well as solving a matrix equation of $3 \times N$ elements in order to provide location estimates. Three equations must be solved by closed-form calculations, to provide the three-axis orientation.

V. Location-Orientation System

This section describes the prototype system. Innovations in the design of the system allow the use of compact, cheap, and commercially available piezoelectric and MEMS transducers for broadband ultrasonic signaling and array signal processing.

The prototype is controlled centrally using a digital signal processing (DSP) board from Sundance, model 361A, which includes a C6416 DSP from Texas Instruments. Attached to it are two daughter boards—a SMT377 with eight independent digital to analog converters (DACs) and a SMT317 with an eight-channel analog to digital converter (ADC). Coaxial cables connect the daughter cards to the transmitter and receiver boards. Centralized control is equivalent to having RF synchronization between the BSs and MD.

The transmitter board consists of an amplifier and a piezoelectric transducer, a Prowave 400ST160, which has a bandwidth of 2 kHz, centered at 41 kHz. This bandwidth is insufficient for SS signaling, so modifications were made to increase the bandwidth. The equivalent circuit of a piezoelectric transmitter is defined as a capacitor C_p in parallel with three components: an inductor L_s, a resistor R_s and a capacitor C_s. The voltage in the equivalent circuit can be calculated as

$$\frac{I_m}{V_m}(S) = \frac{\frac{1}{L_s}S}{S^2 + \frac{R_s}{L_s}S + \frac{1}{L_sC_s}} \quad (39)$$

which is equivalent to a bandpass filter. By adding an inductance and a resistor in series, the response of this circuit can be modified, increasing the bandwidth of the passband. Measurements have shown an increment in bandwidth from 2 kHz up to nearly 15 kHz, depending on the inductance and resistor added, as can be seen in Fig. 7. One important consideration is that the resistor should be as small as possible since it is a dissipative component and can lead to a loss in transmitted power.

A major consideration in the design of the sensor array is the sensor separation. The short wavelength of ultrasonic signals in air means that the distance between sensors must be small. In order to avoid spatial aliasing and phase ambiguities in AoA estimation, the distance between sensors should be less than $\lambda/2$. For ultrasonic signals with a maximum frequency of 50 kHz and a typical sound velocity of 343 m/s, the distance between sensors has to be smaller than 3.43 mm which is impossible to achieve with conventional ultrasonic sensors. Consequently, acoustic sensors based on MEMS technology were used that have a length of 4.72 mm and a width of 3.76 mm and a flat frequency response between 10 and 65 kHz [41]. A footprint plot and picture of the eight element array footprint can be seen in Fig. 8. As can be seen in the figure, the sensor separation is 4.15 mm, allowing for a maximum frequency [32] of $f = c/(2d) = 41.4$ kHz where c is the sound velocity and d the distance between sensors.

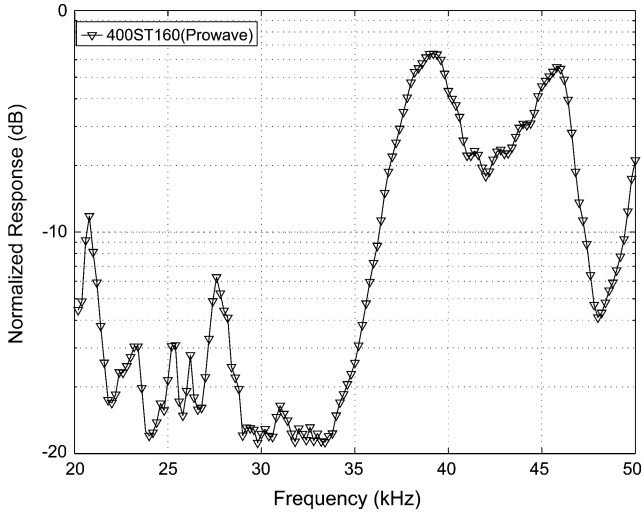

Fig. 7. Frequency response of the channel, including the transducers.

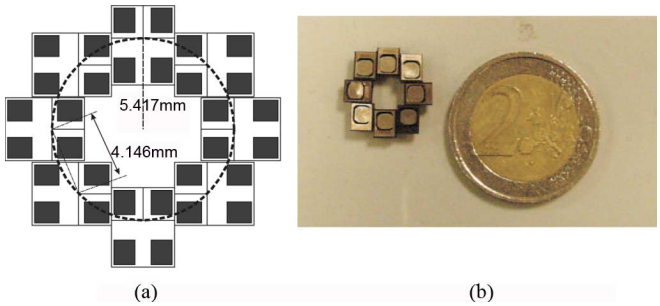

Fig. 8. Sensor array. (a) Footprint. (b) Implementation.

VI. Results

This section presents the results obtained using the proposed system. The section describes the system's accuracy and robustness in ToF and AoA estimation. This is followed by an assessment of its performance in location and orientation estimation. All tests were conducted in a normal office environment in a room $2 \times 4 \times 2$ m in size. No attempt was made to reduce airflow, noise, or reverberation.

In the first set of experiments, the accuracy of ToF estimation was assessed. First, the performance of the various signaling schemes, impulsive, DSSS, and FHSS, was compared. In the case of DSSS and FHSS, a carrier frequency of 40 kHz was used with a bandwidth of 15 kHz. In both cases, Kasami codes were used. DSSS employed 200 symbols with a symbol length of 1/10000 s and 4 carrier cycles per symbol. For FHSS,

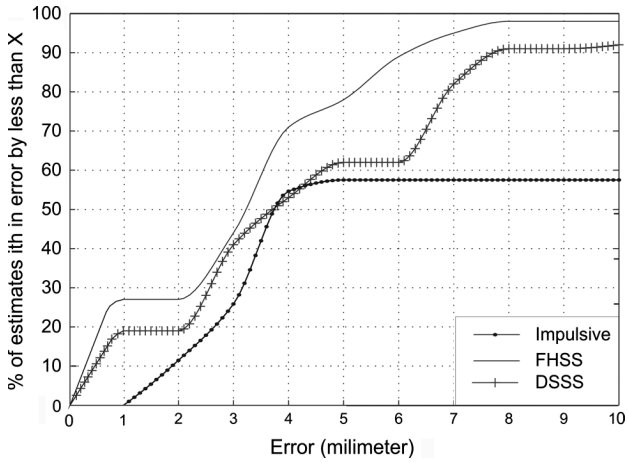

Fig. 9. Cumulative time-of-flight error for FHSS and DSSS and impulsive signalling.

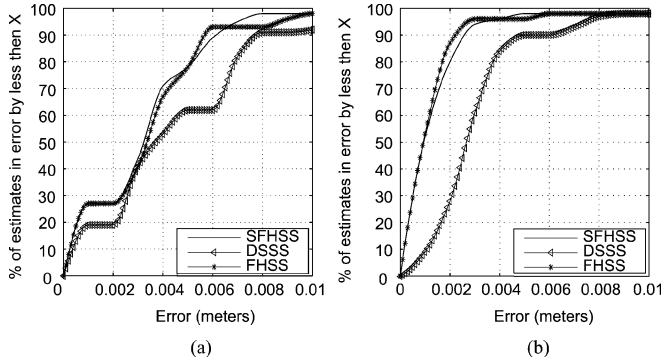

Fig. 10. Cumulative time-of-flight error for various SS modulations. (a) Without complex envelope and interpolation. (b) With complex envelope and interpolation.

50 symbols were used with a symbol length of 1/2500. Six hopping frequencies were used, starting at 33.75 kHz and ending at 46.25 kHz, spaced at intervals of 2.5 kHz. For the Slow-FHSS modulation, 1 hop per 5 symbols were used, and for FHSS 1 hop per symbol was used. The duration of all the signals was 20 ms. Impulsive signalling was performed using a pulse with carrier frequency of 40 kHz and a duration of 400 cycles. Impulsive signalling was introduced because was used in some previous location systems as [12], [13].

Fig. 9 shows the cumulative error in ToF estimation in all three cases. A set of 40 different locations were tested, with 3 estimates per location. The error was calculated by comparing with the measured distances, which had a typical error of 2 mm relative to ground truth. FHSS outperforms DSSS in all the cases and the impulsive signal shows much worse performance in the tests than the spread spectrum modulations, as was expected.

Fig. 10 shows the performance of the system for DSSS, FHSS, and Slow FHSS modulations. Fig. 10(a) presents the ToF cumulative error obtained without using the complex-envelope of the received signals and interpolation. Fig. 10(b) shows the same study using the complex-envelope and interpolation. As can be seen, Slow-FHSS and FHSS outperform DSSS in both cases. The complex envelope and interpolation techniques clearly improve accuracy. FHSS is slightly better than Slow FHSS because the

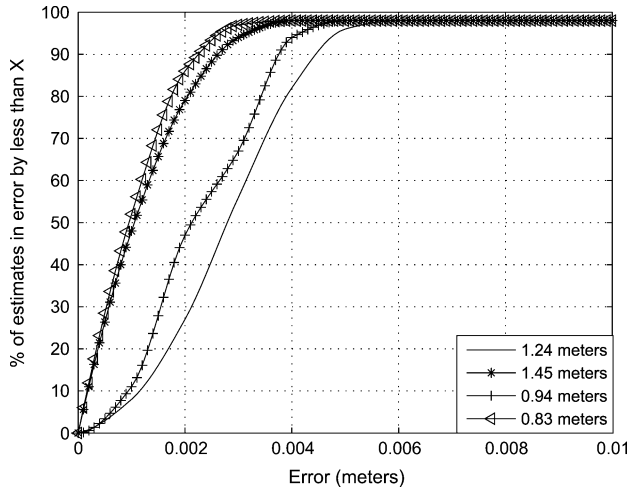

Fig. 11. Variation of cumulative error with range.

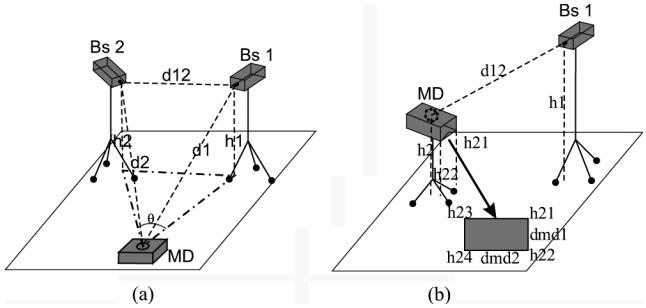

Fig. 12. Angle estimation method.

increased number of hops allows better multipath rejection. The testing conditions were the same as in than Fig. 9. Based on these results from this point on, the modulation used is Fast-FHSS with complex-envelope computation and interpolation, because it was shown that it provides the best results.

Fig. 11 shows how the accuracy of FHSS varies with range. A set of source-receiver distances were tested with 100 estimates at each location. The cumulative error for every location tested was plotted. As can be seen, 95% of estimates have an error of less than 2.7 mm at short range. This rises to 4.7 mm for long ranges. The error at short ranges is mainly due to ground truth errors in the real measurements. The increase in error with range is due to attenuation of the received signal, inaccuracies in temperature measurement and airflow.

The next set of experiments assessed AoA estimation accuracy. The main problem in assessing angle estimation accuracy is in obtaining accurate measurements of the real angles. For the experiments presented herein, two methods were used, one for elevation and another for azimuth. The methods are shown in Fig. 12. Obtaining the absolute azimuth is not as accurate as obtaining the relative azimuth, i.e., the azimuth of one signal relative to another as shown in Fig. 12(a). The estimated angle θ is calculated as follows:

$$\theta = a\cos\left(\frac{d_{12}^2-(d_1\cos(h_1-h_{md}))^2-(d_2\cos(h_2-h_{md}))^2}{-2d_1\cos\left(\frac{h_1-h_{md}}{d_1}\right)d_2\cos\left(\frac{h_2-h_{md}}{d_2}\right)}\right) \quad (40)$$

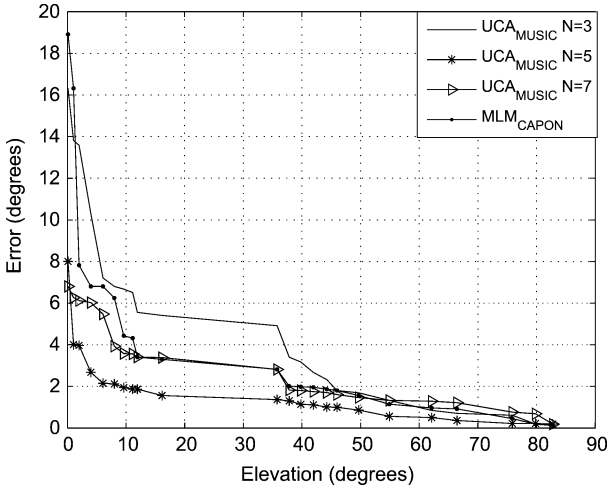

Fig. 13. Elevation error obtained using UCA-MUSIC and MLM Capon.

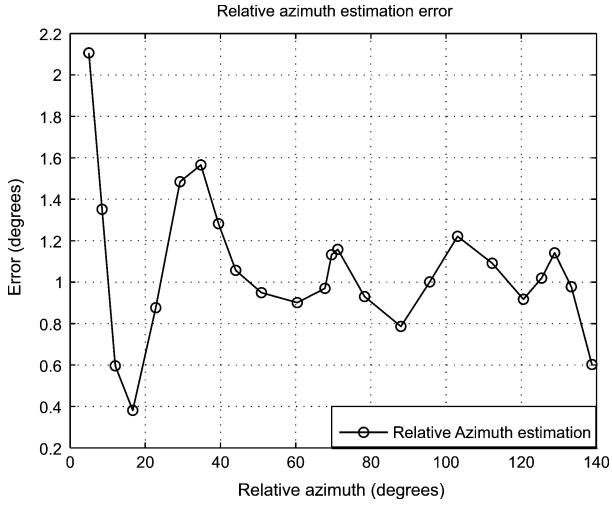

Fig. 14. Azimuth error variation for UCA-MUSIC with $N = 5$.

where d_{12} is the distance between transmitters, h_1 and h_2 are the heights, respectively, of BS_1 and BS_2, d_1 and d_2 are the distances to the receiver from BS_1 and BS_2, and h_{md} is the MD height. Assuming an error in distance measurements of 2 mm, the ground truth error for the azimuth estimation is 0.53°, calculated by obtaining the mean over 2000 simulated estimates.

Elevation is calculated as

$$\phi = a\sin\left(\frac{h1-h2}{d12}\right)$$
$$\varphi_1 = a\sin\left(\frac{abs(h21-h22)}{dmd1}\right) \tag{41}$$

where $h1$ is the BS height, $h2$ the MD height, $d12$ the distance BS-MD, $h21$ and $h22$ are the heights at two of the corners of the MD, and $dmd1$ is the distance between those corners. The signal elevation, provided by ϕ, is compensated with the own elevation of the MD, provided by φ. The ground truth error for the elevation estimation is 1.57° for an error in distance measurement of 2 mm.

The BSs were placed at $[3.6, 0, 1.52]$ and $[3.6, 1.8, 1.52]$ initially. The second BS was rotated to provide various azimuth configurations. The MD was placed at the center of the room, at $[1.8, 0.9, 0.56]$. The height of the receiver was chosen to be low to keep a relative height to the BSs of 1 m.

Fig. 13 shows the elevation error obtained using UCA-MUSIC with N, the number of excitable harmonics fixed to 5, for discrete elevation values averaged over ten estimates per angle. Values were provided by changing the relative heights of the MD and BS because the goal was finding accuracy of the AoA estimation. The N value was calculated using the procedure explained in Section III-B. Results are compared with estimates obtained using MLM Capon [28], a typical beamforming method. Clearly, UCA-MUSIC outperforms MLM Capon when the correct value for N is used.

Fig. 14 shows the accuracy of the method for azimuth estimation. The method was the same as the previous one, using several discrete values, each value shown is the mean error obtained over ten tests. The results are more accurate than those obtained for elevation estimation. As is explained in the literature [31], [32], arrays provide accurate azimuth estimates but less accurate elevation estimates, as can be seen in Fig. 15, where elevation and azimuth estimates are plotted for different SNR values. The azimuth information is extracted from the absolute value of the autovalues of the covariance matrix (Section III-B), whereas the elevation information is obtained from the phase of the autovalues, which is more sensitive to errors in frequency and array calibration.

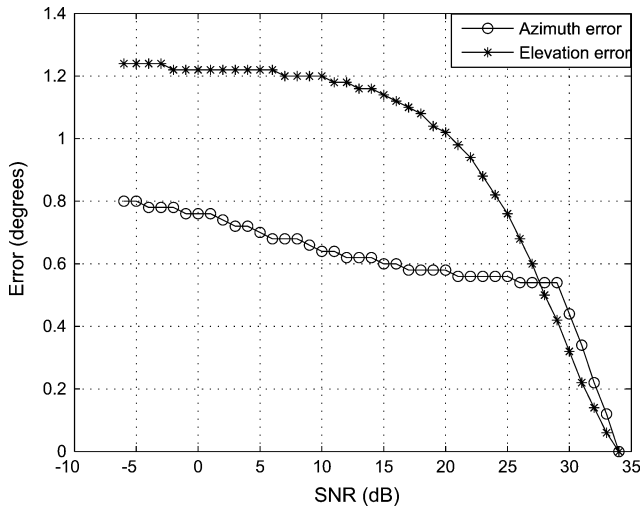

Fig. 15. Elevation and azimuth error versus SNR

The errors in AoA estimation are due to mismatches between the sensors, positioning errors, mutual coupling between the receiver electronics, and the far field assumption. For a source-receiver distance of 2 m and a maximum frequency of 50 kHz, the error expected due to the far-field assumption is one tenth of the wavelength.

Orientation estimation accuracy was assessed by placing the MD in a fixed location and rotating it over the three axis using a tripod. Yaw was calculated by measuring the distance from two corners of the prototype to a reference wall. Roll and pitch were calculated using (41). As before, several discrete orientations were assessed using ten estimates per configuration and the mean error was plotted.

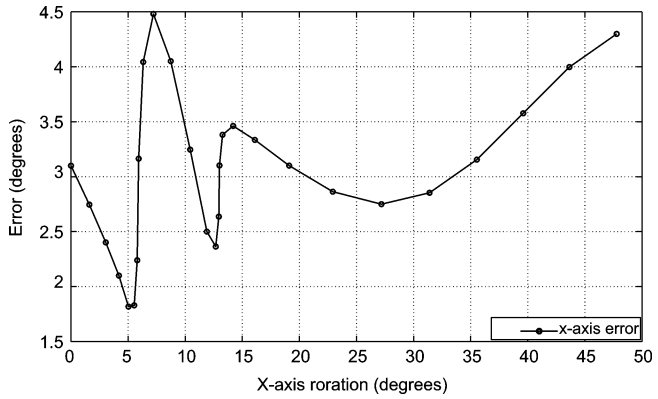

Fig. 16. Accuracy over pitch orientation estimated.

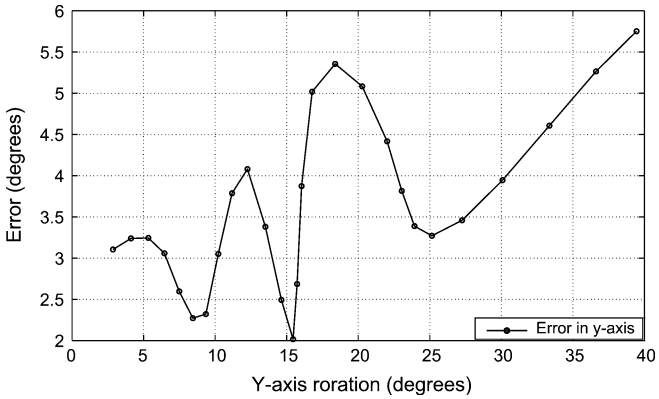

Fig. 17. Accuracy over roll orientation estimated.

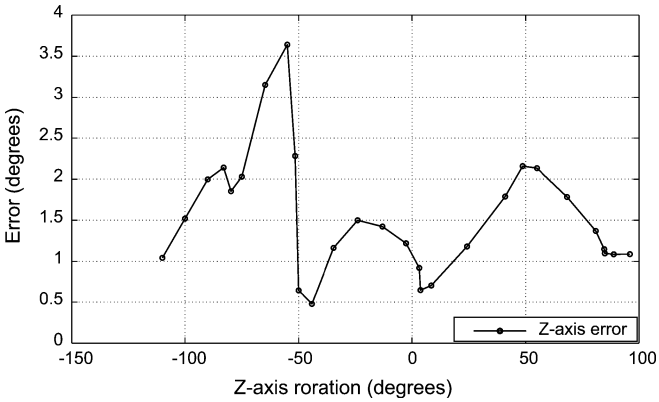

Fig. 18. Accuracy over yaw orientation estimated.

The tests were performed between 0° and 40°–45° because larger angles caused occlusion of one of the BSs. As can be seen in Figs. 16 and 17, the error is uniform over the range, except for values close to the occluding angle where the error increases. The mean error is around 3.5°. Fig. 18 shows the accuracy of yaw estimation. In this case, the mean error is around 1.5°. The difference in mean accuracy arises because estimation of the pitch and yaw is more dependent on the elevation angle which is less accurate than azimuth estimation.

A location accuracy study was conducted by placing three BSs in the corners of the room at positions $[3.6, 0, 1.52]$, $[3.6, 1.8, 1.52]$, and $[0, 1.8, 1.52]$, as can be seen in Fig. 19. Two

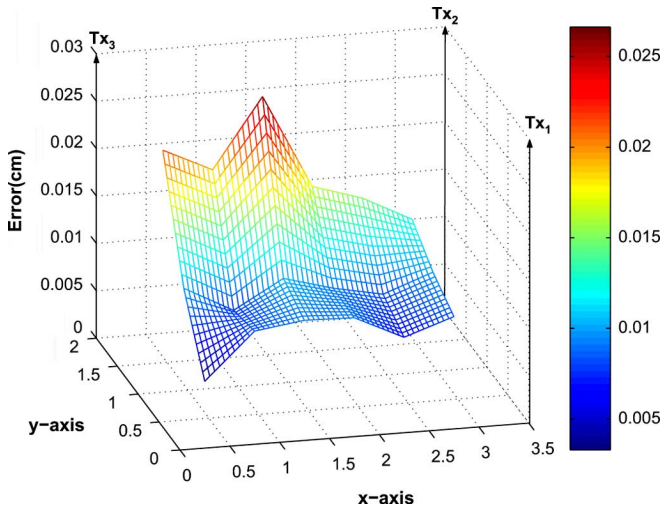

Fig. 19. Location error surface.

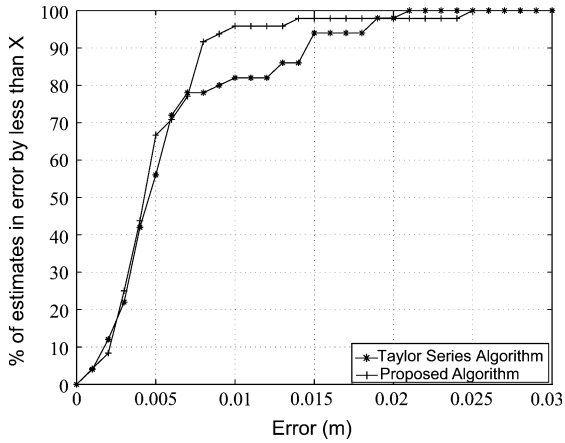

Fig. 20. Location Cumulative error.

studies were conducted. In both studies the transmitters were transmitting simultaneously. The room was empty except for a couple of computers placed at $[1.8, 1.4, 1.2]$ and desks in the corners of the room. Fig. 19 shows a surface plot of the error obtained at discrete locations, averaged over 20 estimates. The MD was placed at a height of 56 cm because the BS's heights were 1.52 m, providing a difference of heights of roughly 1 m, which is typical for real world applications. The mean error surface is very flat, around 1 cm in all cases except for locations close to the computers in the room, where some of the BSs were partially occluded, increasing the error up to 3 cm.

Fig. 20 shows the cumulative error obtained over 100 location estimates, using ten discrete locations and ten estimates per location, for the typical Taylor series based trilateration algorithm compared with the proposed location-orientation algorithm. The Taylor series algorithm only uses one sensor and ToF information. As can be seen, both methods provide good estimates. However, the proposed method is slightly more robust in the tests since it uses a circular sensor array with eight receivers and an estimation error at one sensor is compensated by the others. The proposed method provides an error of less than 1 cm in 95% of cases.

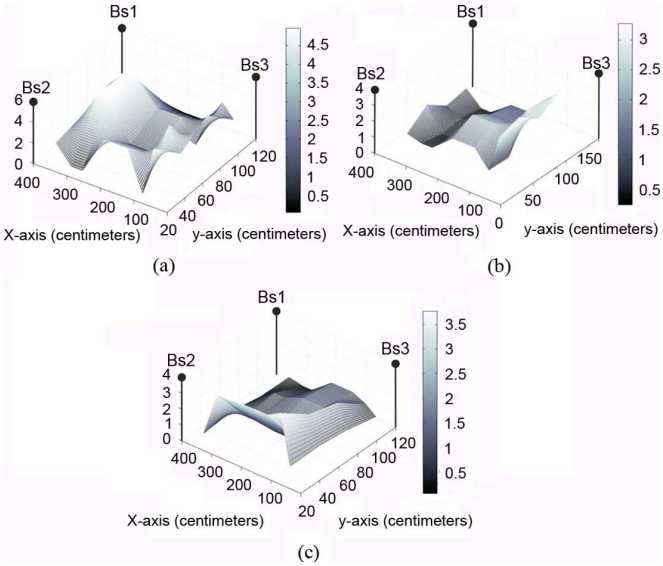

Fig. 21. Orientation error surface: (a) yaw; (b) pitch; (c) roll.

Fig. 21 shows the mean error surface in the tested room for yaw, pitch and roll. Fifty-six points were tested within the room. The ground truth error was 1° per axis. BSs were placed in the same locations and the testing conditions were the same as for the results in Fig. 20. It can be seen that the algorithm performs better for central points in the room, as was expected from the Geometric Dilution of Precision (DoP). The maximum errors were 4.5°, 3°, and 3.5° in yaw, pitch, and roll, respectively.

VII. Conclusion

A novel location and orientation system has been proposed. The performance of the system has been established by means of a prototype operating in a real office environment. The results show a 3-D location error of less than 1 cm in 95% of cases as well as three-axis orientation estimation with a mean error of 4.5° in yaw, 3° in pitch, and 3.5° in roll.

As well as the proposed algorithms, the electronic prototype used to verify them has been presented. The prototype uses modified piezoelectric transmitters to generate broadband signals and new MEMs sensors. Use of these sensors is significant since their small size enables the use of array signal processing methods for AoA estimation in the ultrasonic range.

During system characterization, some points of non-convergence were found in 4% of cases between 180° and 360° in yaw. Although these errors are tolerable, a further study will be performed to find the source of the problem. A modified AoA estimation algorithm will be developed in order to compensate for errors arising due to the far field assumption. It is expected that development of a printed circuit board for the receiver signal conditioning electronics will improve system performance by reducing mutual coupling between channels in the receiver.

References

[1] I. Korhonen, P. Paavilainen, and A. Sarela, "Application of ubiquitous computing technologies for support of independent living of the elderly," in *Proc. 2nd Int. Workshop Ubiquitous Comput. Pervasive Healthcare Applicat.*, Seattle, WA, 2003, pp. 28–40.

[2] G. D. Abowd and E. D. Mynatt, "Charting past, present, and future research in ubiquitous computing," *ACM Trans. Comput.-Human Interaction (TOCHI)*, vol. 7, no. 1, pp. 29–58, 2000.

[3] A. Smith, H. Balakrishnan, M. Goraczko, and N. B. Priyantha, "Tracking moving devices with the cricket location system," *Proc. 2nd Int. Conf. Mobile Syst., Applicat., Services*, pp. 190–202, 2004.

[4] C. R. Wren, A. Azarbayejani, T. Darrell, and A. P. Pentland, "Pfinder: Real-time tracking of the human body," *IEEE Trans. Pattern Anal Mach. Intell.*, vol. 19, no. 7, pp. 780–785, Jul. 1997.

[5] M. Deering, "High resolution virtual reality," in *Proc. 19th Annu. Conf. Comput. Graph. Interactive Tech.*, 1992, pp. 195–202.

[6] C. Hand, "A survey of 3D interaction techniques," *Comput. Graph. Forum*, vol. 16, no. 5, pp. 269–281, 1997.

[7] J. J. Leonard and H. F. Durrant-Whyte, "Mobile robot localization by tracking geometric beacons," *IEEE Trans. Robot. Autom.*, vol. 7, no. 3, pp. 376–382, Jun. 1991.

[8] J. R. Gonzalez and C. J. Bleakley, "Ultrasonic orientation-location algorithm based on time and angle of arrival measurements," in *Proc. IEEE 10th Int. Symp. Spread Spectrum Tech. Applicat. (ISSSTA)*, Bologna, Italy, 2008, pp. 800–805.

[9] A. Falsafi and K. Pahlavan, "A comparison between the performance of FHSS and DSSS for wirelessLANs using a 3D ray tracing program," in *Proc. IEEE 45th Veh. Technol. Conf.*, 1995, vol. 2, pp. 569–573.

[10] C. P. Mathews and M. D. Zoltowski, "Eigenstructure techniques for 2-D angle estimation with uniformcircular arrays," *IEEE Trans. Signal Process.*, vol. 42, no. 9, pp. 2395–2407, Sep. 1994.

[11] C. P. Mathews and M. D. Zoltowski, "Location systems for ubiquitous computing," *Computer*, vol. 34, no. 8, pp. 57–66, Aug. 2001.

[12] A. Harter, A. Hopper, P. Steggles, A. Ward, and P. Webster, "The anatomy of a context-aware application," *Wireless Networks, Spinger-Verlag*, vol. 8, no. 2–3, pp. 187–197, 2002.

[13] N. B. Priyantha, A. Chakraborty, and H. Balakrishnan, "The cricket location-support system," in *Proc. 6th ACM MOBICOM*, Aug. 2000, pp. 32–43.

[14] M. Hazas and A. Hopper, "Broadband ultrasonic location systems for improved indoor positioning," *IEEE Trans. Mobile Comput.*, vol. 5, pp. 536–547, May 2006.

[15] M. Hazas and A. Hopper, "A novel broadband ultrasonic location system," in *Lecture Notes in Computer Science*. New York: Springer, 2002, pp. 264–280.

[16] N. M. Vallidis, *WHISPER: A Spread Spectrum Approach to Occlusion in Acoustic Tracking*. Chapel Hill, NC: Univ. of North Carolina at , Dept. of Comput. Sci., 2002.

[17] W. Jung, W. Woo, and S. Lee, "Orientation tracking exploiting ubi-Track," in *Proc. 7th Annu. Int. Conf. Mobile Comput. Netw.*, 2001, pp. 1–14.

[18] N. B. Priyantha, A. K. L. Miu, H. Balakrishnan, and S. Teller, "The cricket compass for context-aware mobile applications," in *Proc. 7th ACM MOBICOM*, Jul. 2001, pp. 1–14.

[19] L. Baillie, H. Kunczier, and H. Anegg, "Rolling, rotating and imagining in a virtual mobile world," in *Proc. 7th Int. Conf. Human Comput. Interaction With Mobile Devices Services*, 2005, pp. 283–286.

[20] K. Hinckley, J. Pierce, M. Sinclair, and E. Horvitz, "Sensing techniques for mobile interaction," in *Proc. 13th Annu. ACM Symp. User Interface Software Technol.*, 2000, pp. 91–100.

[21] E. H. Thompson, "An exact linear solution of the problem of absolute orientation," *Photogrammetria*, vol. 14, no. 8, pp. 20–28, 1959.

[22] G. H. Schut, "On exact linear equations for the computation of the rotational elements of absolute orientation," *Photogrammetria*, vol. 17, no. 1, pp. 34–37, 1960.

[23] F. Sans, "An exact solution of the roto-translation problem," *Photogrammetria*, vol. 29, pp. 203–216, 1973.

[24] B. K. P. Horn, "Closed-form solution of absolute orientation using unit quaternions," *J. Opt. Soc. Amer.*, pp. 629–642, 1987.

[25] B. Horn, H. Hilden, and S. Negahdaripour, "Closed-form solution of absolute orientation using orthonormal matrices," *J. Opt. Soc. Amer.*, vol. 5, no. 7, pp. 1127–1135, 1988.

[26] D. Torrieri, *Princpiles of Spread Spectrum Communication Systems*. New York: Springer, 2005.

[27] K. Fazel, S. Kaiser, and I. NetLibrary, *Multicarrier and Spread Spectrum Systems*. New York: Wiley, 2005.

[28] C. Kyungwhoon, "Performance of the limiter-discriminator-integrator detector in frequency-hop spread-spectrum multiple-access networks," *IEEE Commun. Lett.*, vol. 1, pp. 121–123, Sep. 1997.

[29] J. H. Gass, Jr, M. B. Pursley, C. Div, I. T. T. Aerosp, and S. C. Pendleton, "A comparison of slow-frequency-hop and direct-sequencespread-spectrum systems for different multipath delay profiles," *Proc. MILCOM 97*, vol. 2, pp. 812–816, Nov. 1997.

[30] D. Colton and R. Krees, *Inverse Acoustic and Electromagnetic Scattering Theory*, 2nd ed. New York: Springer, 1998.
[31] H. L. Van Trees, *Optimum Array Processing—Part IV of Detection, Estimation and Modulation Theory*. New York: Wiley-Interscience, 2002.
[32] H. Krim, M. Viberg, and C. Mit, "Two decades of array signal processing research," *IEEE Signal Process. Mag.*, vol. 13, no. 4, pp. 67–94, Jul. 1996.
[33] J. G. Davis and A. A. P. Gibson, "Phase mode excitation in beamforming arrays," in *Proc. 3rd Eur. Radar Conf., EuRAD'06*, Sep. 2006, pp. 307–310.
[34] J. R. Gonzalez and C. J. Bleakley, "Accuracy of spread spectrum techniques for ultrasonic indoor location," in *Proc. 15th Int. Conf. Digital Signal Process.*, Jul. 2007, vol. 1, pp. 284–287.
[35] R. T. Barghouthi and G. L. Stuber, "Rapid sequence acquisition for DS/CDMA systems employing Kasami sequences," *IEEE Trans. Commun.*, vol. 42, no. 2/3/4, pp. 1957–1968, Feb./Mar./Apr. 1994.
[36] G. Mazzini, "DS-CDMA systems using q-level m sequences: Coding map theory," *IEEE Trans. Commun.*, vol. 45, no. 10, pp. 1304–1313, Oct. 1997.
[37] O. S. Rothaus, "Modified gold codes," *IEEE Trans. Inf. Theory*, vol. 39, no. 2, pp. 654–656, Mar. 1993.
[38] Y. Li and W. B. Chu, "More Golay sequences," *IEEE Trans. Inf. Theory*, vol. 51, no. 3, pp. 1141–1145, Mar. 2005.
[39] M. I. Skolnik, *Radar Handook*. New York: McGraw-Hill, 1970.
[40] W. H. Foy, "Position-location solutions by Taylor-series estimation," *IEEE Trans. Aerosp. Electron. Syst.*, vol. AES-12, no. 2, pp. 187–194, Mar. 1976.
[41] SPM0204UD5 MEMS Acoustic Sensor, [Online]. Available: http://www.knowles.com
[42] J. R. Gonzalez and C. J. Bleakley, "Robust 3D orientation-location estimation for ultrasonic sensor arrays," in *Proc. IEEE Int. Symp. Wireless Pervasive Comput. (ISWPC)*, Santorini, Geece, 2008, pp. 374–378.

J. R. Gonzalez was born in Madrid, Spain, on December 23, 1983. He received the degree in telecommunication engineering from the Universidad de Alcalá (UAH), Madrid, in 2006. He is currently pursuing the Ph.D. degree at University College Dublin, Dublin, Ireland.

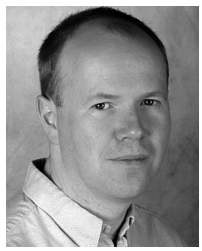

C. J. Bleakley received the first class honors degree in computer science from Queen's University, Belfast, U.K., and the Ph.D. degree from Dublin City University, Dublin, in 1995.

He is a Lecturer in the School of Computer Science and Informatics, University College Dublin (UCD), Dublin, Ireland. After graduation, he worked as Researcher with Broadcom Eireann Research, Ltd., a research organization jointly owned by Ericsson, Eircom, and Trinity College Dublin. Prior to joining UCD in November 2003, he was Vice-President of Engineering with Massana, Ltd.